Neutrino-deuteron scattering in effective field theory at next-to-next-to-leading order

Malcolm Butler*
Department of Astronomy and Physics, Saint Mary's University, Halifax, Nova Scotia, Canada B3H 3C3

Jiunn-Wei Chen†
Department of Physics, University of Maryland, College Park, Maryland 20742

Xinwei Kong‡
TRIUMF, 4004 Wesbrook Mall, Vancouver, British Columbia, Canada V6T 2A3

(Received 20 October 2000; published 21 February 2001)

We study the four channels associated with neutrino-deuteron breakup reactions at next-to-next-to-leading order in effective field theory. We find that the total cross section is indeed converging for neutrino energies up to 20 MeV, and thus our calculations can provide constraints on theoretical uncertainties for the Sudbury Neutrino Observatory. We stress the importance of a direct experimental measurement to high precision in at least one channel, in order to fix an axial two-body counterterm.

DOI: 10.1103/PhysRevC.63.035501 PACS number(s): 25.30.Pt, 13.75.Cs, 12.15.Ji, 27.10.+h

I. INTRODUCTION

Our understanding of electroweak processes on the deuteron is reaching a critical juncture. The Sudbury Neutrino Observatory is taking data, and a thorough understanding of neutrino-deuteron scattering is an important part of the analysis in that experiment [1,2]. Of further note, there is a proposal for a high-precision measurement of the reaction $\nu_e d \to e^- pp$ in the ORLaND facility [3].

Theorists have made a tremendous effort to understand $\nu(\bar{\nu})-d$ scattering in a potential model framework [4–10], with the most recent independent efforts agreeing within a few percent at low energy [11,12]. Given the ongoing experimental interest in these processes, efforts began to study $\nu(\bar{\nu})-d$ scattering in the language of effective field theory (EFT) [13] for neutrino energies below 20 MeV. The EFT work employed the power-counting scheme of Kaplan, Savage, and Wise [14] and included pions. In working to next-to-leading order (NLO), it was found in Ref. [13] that theoretical uncertainties in the reactions $\nu d \to \nu np$, $\bar{\nu} d \to \bar{\nu} np$, and $\bar{\nu}_e d \to e^+ nn$ were dominated by an unknown axial two-body counterterm $L_{1,A}$. It was possible to find different values of $L_{1,A}$ which provided excellent fits to the potential model calculations of Refs. [10,11]. Further, we found that the ratio of charged current to neutral current (CC/NC) cross sections was insensitive to this counterterm. This confirmed the insensitivity to short-distance physics first discussed by Ref. [11]. However, it is not clear whether a power-counting scheme exists which would allow us to extend the theory with pions to higher order [15–18], as would be required to constrain our theoretical uncertainties.

In this work, we employ the theory without pions [19] (see also earlier works [14,20–26]) which has proven so successful in providing for high-precision calculations for other processes like $np \to d\gamma$ [27,28]. This allows us to consider next-to-next-to-leading order (NNLO) corrections, and to incorporate Coulomb effects cleanly, following the prescription of Kong and Ravndal [29] with some generalization. As a result, we present a complete set of calculations for all four reaction channels including the most important pp channel. No new parameters are introduced at this order, so it becomes a stringent test of the convergence of the calculation and thus on the theoretical uncertainties. Further, new potential model calculations exist [12] and a comparison to those is worthwhile, given that these new calculations yield different results at threshold to those in Ref. [10]. We continue to emphasize the importance of fixing the axial counterterm through a direct experimental measurement. This has implications not only for neutrino-deuteron scattering, but also for $pp \to de^+ \nu_e$, $NN \to NN\bar{\nu}\nu$, and parity violating $\vec{e}-d$ scattering.

II. THE LAGRANGIAN

We will briefly review nuclear effective field theory without pions [19]. The dynamical degrees of freedom are nucleons and nonhadronic external currents. Massive hadronic excitations such as pions and the delta are treated as nondynamical, point interactions whose effects are encoded in the local operators in the Lagrangian. The nucleons are nonrelativistic but relativistic corrections are built in systematically. Nuclear interaction processes are calculated perturbatively with the small expansion parameter

$$Q \equiv \frac{(1/a, \gamma, p, |\mathbf{q}|)}{\Lambda} \tag{1}$$

which is the ratio of the light to heavy scales. The light scales include the inverse S-wave nucleon-nucleon scattering length $1/a (\lesssim 12$ MeV) in the $^1S_0$ channel, the deuteron binding momentum $\gamma (= 45.69$ MeV) in the $^3S_1$ channel, the magnitude of the nucleon external momentum p in the two

*Electronic address: mbutler@ap.stmarys.ca
†Electronic address: jwchen@physics.umd.edu
‡Electronic address: kong@alph01.triumf.ca

nucleon center-of-mass frame, and the momentum transfer to the two nucleon system $|\mathbf{q}|$. The heavy scale Λ is set by the pion mass m_π. How each term in the Lagrangian scales as powers of Q can be found in Ref. [19]. It is the nontrivial renormalization of the strong interaction operators makes the scaling different from a naive derivative expansion [14].

A. The effective Lagrangian

The Lagrangian of an effective field theory for nucleons can be described via

$$\mathcal{L}=\mathcal{L}_1+\mathcal{L}_2+\cdots, \tag{2}$$

where $\mathcal{L}_n$ contains operators involving n nucleons. Neglecting for the moment the weak-interaction couplings, we have

$$\mathcal{L}_1=N^\dagger\left(iD_0+\frac{\mathbf{D}^2}{2M_N}-\frac{D_0^2}{2M_N}\right)N, \tag{3}$$

where N is the nucleon field, M_N is the nucleon mass, D_0 and $\mathbf{D}$ are covariant derivatives and the D_0^2 term is the leading relativistic correction.

The two-nucleon Lagrangian needed for a calculation to NNLO is

$$\begin{aligned}\mathcal{L}_2=&-C_0^{(^3S_1)}(N^TP_iN)^\dagger(N^TP_iN)+\frac{C_2^{(^3S_1)}}{8}[(N^TP_iN)^\dagger\\&\times(N^T(\tilde{\mathbf{D}}^2P_i-2\tilde{\mathbf{D}}\cdot P_i\vec{\mathbf{D}}+P_i\vec{\mathbf{D}}^2)N)+\text{H.c.}]\\&-\frac{C_4^{(^3S_1)}}{16}(N^T[P_i\vec{\mathbf{D}}^2+\tilde{\mathbf{D}}^2P_i-2\tilde{\mathbf{D}}P_i\vec{\mathbf{D}}]N)^\dagger\\&\times(N^T[P_i\vec{\mathbf{D}}^2+\tilde{\mathbf{D}}^2P_i-2\tilde{\mathbf{D}}P_i\vec{\mathbf{D}}]N)-C_0^{(^1S_0,i)}(N^T\overline{P}_iN)^\dagger\\&\times(N^T\overline{P}_iN)+\frac{C_2^{(^1S_0,i)}}{8}[(N^T\overline{P}_iN)^\dagger(N^T(\tilde{\mathbf{D}}^2\overline{P}_i-2\tilde{\mathbf{D}}\cdot\overline{P}_i\vec{\mathbf{D}}\\&+\overline{P}_i\vec{\mathbf{D}}^2)N)+\text{H.c.}]-\frac{C_4^{(^1S_0,i)}}{16}(N^T[\overline{P}_i\vec{\mathbf{D}}^2+\tilde{\mathbf{D}}^2\overline{P}_i\\&-2\tilde{\mathbf{D}}\overline{P}_i\vec{\mathbf{D}}]N)^\dagger(N^T[\overline{P}_i\vec{\mathbf{D}}^2+\tilde{\mathbf{D}}^2\overline{P}_i-2\tilde{\mathbf{D}}\overline{P}_i\vec{\mathbf{D}}]N),\end{aligned} \tag{4}$$

where P_i and $\overline{P}_i$ are spin–isospin projectors for the $^3S_1$ channel and the $^1S_0$ channel, respectively,

$$\begin{aligned}P_i&\equiv\frac{1}{\sqrt{8}}\sigma_2\sigma_i\tau_2, \quad \mathrm{Tr}\,P_i^\dagger P_j=\tfrac{1}{2}\delta_{ij},\\ \overline{P}_i&\equiv\frac{1}{\sqrt{8}}\sigma_2\tau_2\tau_i, \quad \mathrm{Tr}\,\overline{P}_i^\dagger\overline{P}_j=\tfrac{1}{2}\delta_{ij},\end{aligned} \tag{5}$$

where τ matrices act on isospin indices and σ matrices on the spin indices. We incorporate isospin symmetry breaking in the $C_{2n}^{(^1S_0,i)}(n=0,1,\ldots)$ operators, so that $C_{2n}^{(^1S_0,pp)}$, $C_{2n}^{(^1S_0,np)}$, and $C_{2n}^{(^1S_0,nn)}$ are different. In both the $^3S_1$ and $^1S_0$ channels, the strong coupling constants C_{2n} have renormalization scale (μ) dependence. These parameters can be fit to the effective range expansion, as detailed in Ref. [19] and as reviewed in Appendix A.

Relativistic corrections start to contribute to physical quantities at NNLO and have generic sizes of $\mathcal{O}(p^2/m_N^2)$ of the leading-order (LO) contribution (see Ref. [19] for examples). They are suppressed by an additional factor of Λ^2/m_N^2 to other NNLO contributions, and thus we can neglect them as small (this is verified numerically).

B. Weak interactions

The effective Lagrangians for charged (CC) and neutral current (NC) weak interactions are given by

$$\mathcal{L}^{\mathrm{CC}}=-\frac{G_F}{\sqrt{2}}l_+^\mu J_\mu^-+\text{H.c.}, \tag{6}$$

$$\mathcal{L}^{\mathrm{NC}}=-\frac{G_F}{\sqrt{2}}l_Z^\mu J_\mu^Z, \tag{7}$$

where the l_μ is the leptonic current and J_μ is the hadronic current. We have used $G_F=1.166\times10^{-5}$ GeV^{-2}. For $\nu-d$ and $\overline{\nu}-d$ scattering,

$$l_+^\mu=\overline{\nu}\gamma^\mu(1-\gamma_5)e, \quad l_Z^\mu=\overline{\nu}\gamma^\mu(1-\gamma_5)\nu. \tag{8}$$

The hadronic currents can be decomposed into vector and axial-vector contributions

$$\begin{aligned}J_\mu^-&=V_\mu^--A_\mu^-=(V_\mu^1-A_\mu^1)-i(V_\mu^2-A_\mu^2),\\ J_\mu^Z&=-2\sin^2\theta_WV_\mu^S+(1-2\sin^2\theta_W)V_\mu^3-A_\mu^S-A_\mu^3,\end{aligned} \tag{9}$$

where the superscripts represent isovector components (with S representing isoscalar terms) and, later, the currents will be labeled by the number of nucleons involved.

In a NNLO calculation, the electron mass m_e contributions to the matrix elements are counted as higher order (suppressed by a factor of m_e^2/γ^2), such that $q_\mu l^\mu=0$ up to NNLO. Similarly, if the neutrino mass $m_\nu\neq0$ but $m_\nu^2/\gamma^2\ll1$, then the massless neutrino treatment we have here is still applicable. The nonrelativistic one-body currents are given by

$$V_0^{(1)}=\tfrac{1}{2}N^\dagger(1+\tau_a)N,$$

$$A_0^{(1)}=-\frac{i}{2}N^\dagger(\Delta s-g_A\tau_a)\frac{\sigma\cdot(\vec{\tilde{\nabla}}-\vec{\nabla})}{2M_N}N,$$

$$V_k^{(1)}=\frac{i}{2}N^\dagger(1+\tau_a)\frac{(\vec{\tilde{\nabla}}_k-\vec{\nabla}_k)}{2M_N}N-N^\dagger \tag{10}$$

$$\times\left(\kappa^{(0)}+\frac{\mu_s}{4\sin^2\theta_W}+\kappa^{(1)}\tau_a\right)\epsilon_{kij}\frac{\sigma_i(\vec{\tilde{\nabla}}_j+\vec{\nabla}_j)}{2M_N}N,$$

$$A_k^{(1)}=-\frac{1}{2}N^\dagger(\Delta s-g_A\tau_a)\sigma_k N,$$

where $g_A=1.26$. Here we have neglected the nucleon vector and axial vector charge radius contributions. They only contribute at NNLO with about the same size as the relativistic contributions due to the small momentum transfers being considered here.

We use the notation Δs for the strange quark contribution to the proton spin

$$2S_\mu\Delta s\equiv\langle p|\bar{s}\gamma_\mu\gamma_5 s|p\rangle \tag{11}$$

with the value [30]

$$\Delta s=-0.17\pm0.17, \tag{12}$$

where S_μ is the covariant spin vector. $\kappa^{(0)}=\frac{1}{2}(\kappa_p+\kappa_n)$ and $\kappa^{(1)}=\frac{1}{2}(\kappa_p-\kappa_n)$ are the conventional isoscalar and isovector nucleon magnetic moments in nuclear magnetons, with

$$\kappa_p=2.792\,85,\quad \kappa_n=-1.913\,04. \tag{13}$$

μ_s is the strange magnetic moment of the proton [31]

$$\langle p|\bar{s}\gamma_\mu s|p\rangle=\bar{u}_p\left(F_1^s(q^2)\gamma_\mu+F_2^s(q^2)\frac{i\sigma_{\mu\nu}q^\nu}{2M_N}\right)u_p,$$

$$G_M^s(q^2)\equiv F_1^s(q^2)+F_2^s(q^2), \tag{14}$$

$$F_1^s(0)=0,\quad \mu_s\equiv G_M^s(0).$$

In Ref. [32], the sample experiment found

$$G_M^s(-0.1\ \text{GeV}^2)=0.23\pm0.37\pm0.15\pm0.19\ \text{nm}, \tag{15}$$

extracted from the proton target experiment. However, the newest deuteron target measurement suggests that the radiative corrections to the axial form factor were underestimated. Thus the central value of $G_M^s(-0.1\ \text{GeV}^2)$ could be 40% smaller [33]. Theoretical predictions for μ_s itself range from -0.8 nm to 0.8 nm.

Finally, there are two-body currents relevant to this process. As mentioned in Ref. [13], there are axial contributions

$$A_k^{(2)}=L_{1,A}(N^TP_kN)^\dagger(N^T\bar{P}_aN)-2i\varepsilon_{ijk}L_{2,A}$$
$$\times(N^TP_iN)^\dagger(N^TP_jN)+\text{H.c.}, \tag{16}$$

and analogous vector contributions to the deuteron magnetic properties, as described in Refs. [19,14]

$$V_k^{(2)}=e\varepsilon_{kij}L_1(N^TP_iN)^\dagger(\vec{\tilde{\nabla}}_j+\vec{\nabla}_j)(N^T\bar{P}_aN)$$
$$-2ieL_2(N^TP_iN)^\dagger(\vec{\tilde{\nabla}}_i+\vec{\nabla}_i)(N^TP_kN)+\text{H.c.} \tag{17}$$

The parameters L_1 and L_2 can be fit from $np\to d\gamma$ and the deuteron magnetic moment, respectively, and are given by $L_1=7.24$ fm^4 and $L_2=-0.149$ fm^4 at $\mu=m_\pi$ [19].

III. $\nu(\bar{\nu})$-D NEUTRAL CURRENT INELASTIC SCATTERING

For the inelastic scattering process

$$\nu+d\to\nu+n+p, \tag{18}$$

the differential cross section can be written in terms of leptonic and hadronic tensors $l_{\mu\nu}$ and $W_{\mu\nu}$ as

$$\frac{d^2\sigma}{d\omega'\,d\Omega}=\frac{G_F^2|\mathbf{k}'|}{32\pi^2|\mathbf{k}|}S_1(|\mathbf{k}'|)l^{\mu\nu}W_{\mu\nu}, \tag{19}$$

where $\omega(\omega')=k_0(k_0')$ represent the initial (final) neutrino energies

$$S_1(|\mathbf{k}'|)=1 \tag{20}$$

for NC processes. The leptonic tensor is given by

$$l^{\mu\nu}=8(k^\mu k^{\nu'}+k^\nu k^{\mu'}-k\cdot k'g^{\mu\nu}+i\varepsilon^{\mu\nu\rho\sigma}k_\rho k'_\sigma). \tag{21}$$

The hadronic tensor is the imaginary part of the forward matrix element of the time order product of two weak current operators. It can be parametrized by six different structure functions

$$W_{\mu\nu}=\frac{1}{\pi}\text{Im}\left[\int d^4x\,e^{iqx}T\langle d(P)|J_\mu^{Z^\dagger}(x)J_\nu^Z(0)|d(P)\rangle\right]$$
$$=-W_1g_{\mu\nu}+W_2\frac{P_\mu P_\nu}{M_d^2}-iW_3\varepsilon_{\mu\nu\alpha\beta}\frac{P^\alpha q^\beta}{M_d^2}+W_4\frac{q_\mu q_\nu}{M_d^2}$$
$$+W_5\frac{(P_\mu q_\nu+q_\mu P_\nu)}{M_d^2}+iW_6\frac{(P_\mu q_\nu-q_\mu P_\nu)}{M_d^2}, \tag{22}$$

where the momentum transfer $q_\mu=k_\mu-k'_\mu$. We can easily see that W_4, W_5, and W_6 do not contribute to the differential cross section because $q_ul^{\mu\nu}=0$. In the laboratory frame (deuteron rest frame) the differential cross section simplifies to

$$\frac{d^2\sigma}{d\omega'd\Omega}=\frac{G_F^2\omega'|\mathbf{k}'|}{2\pi^2}S_1(|\mathbf{k}'|)\left[2W_1\sin^2\frac{\theta}{2}+W_2\cos^2\frac{\theta}{2}\right.$$
$$\left.-2\frac{(\omega+\omega')}{M_d}W_3\sin^2\frac{\theta}{2}\right], \tag{23}$$

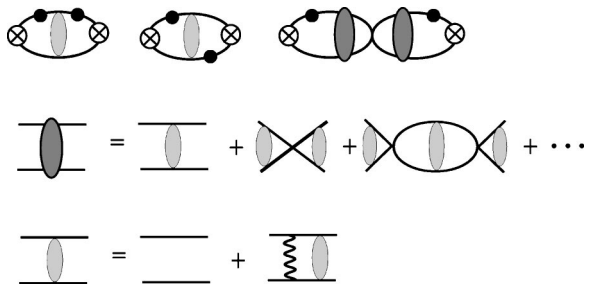

FIG. 1. Diagrams that contribute to W_0 and W_1 at leading order. The crossed circles denote operators that create or annihilate two nucleons with the quantum numbers of the deuteron. The dark gray blobs arise from scattering corrections involving insertions of C_0 operators of the appropriate channel, and from the Coulomb Green's function (the light gray blob). The wavy line represents the Coulomb interaction, present only in the pp final state. Solid lines represent nucleons, and the solid circles represent insertions of electroweak current operators.

where the θ is the angle between $\mathbf{k}$ and $\mathbf{k}'$ and we have used the relation

$$q^2 = -4\omega\omega' \sin^2\frac{\theta}{2}. \tag{24}$$

For $\bar{\nu}d \to \bar{\nu}np$ scattering, the last terms on the right-hand sides of Eqs. (21) and (23) change sign.

Phase space for this reaction is defined by

$$\mathrm{Max}\left[-1, 1-\frac{4M_N(\nu-B)-\nu^2}{2\omega\omega'}\right] \leqslant \cos\theta \leqslant 1 \tag{25}$$

and

$$0 \leqslant \omega' \leqslant \omega - 2(M_N - \sqrt{M_N^2-\gamma^2}), \tag{26}$$

where $\nu=\omega-\omega'$, M_N is the nucleon mass, and B ($=2.2245$ MeV) is the deuteron binding energy. In the deuteron rest frame,

$$W_0 \equiv W_{00} = W_2 - W_1,$$
$$W_{0i} = 0, \tag{27}$$
$$W_{ij} \equiv \delta_{ij} W_1 - i W_3 \varepsilon_{0ijk}\frac{q^k}{M_d}.$$

The structure function can be Q expanded as

$$W_{\mu\nu} = W_{\mu\nu}^{\mathrm{LO}} + W_{\mu\nu}^{\mathrm{NLO}} + W_{\mu\nu}^{\mathrm{NNLO}} + \cdots. \tag{28}$$

Now we give the expressions for the structure functions order by order in the perturbative expansion.

A. Leading order (LO)

The LO diagrams in Fig. 1 give

$$W_0^{\mathrm{LO}} = [2(C_V^{(0)^2} + C_V^{(1)^2})F_1 + (C_V^{(0)^2} - C_V^{(1)^2})F_2 + 4C_V^{(0)^2}F_3^{\mathrm{LO}}],$$
$$W_1^{\mathrm{LO}} = [2(C_A^{(0)^2} + C_A^{(1)^2})F_1 + \tfrac{1}{3}(C_A^{(0)^2} - C_A^{(1)^2})F_2 + \tfrac{8}{3}C_A^{(0)^2}F_3^{\mathrm{LO}} + \tfrac{4}{3}C_A^{(1)^2}F_4^{\mathrm{LO}}], \tag{29}$$
$$W_3^{\mathrm{LO}} = 0.$$

The vector and axial-vector coupling coefficients are given by

$$C_V^{(0)} = -\sin^2\vartheta_W, \quad C_V^{(1)} = \tfrac{1}{2}(1-2\sin^2\vartheta_W),$$
$$C_A^{(0)} = -\tfrac{1}{2}\Delta s, \quad C_A^{(1)} = \tfrac{1}{2}g_A. \tag{30}$$

The structure and interaction effects are contained in

$$F_1 = \frac{2M_N\gamma p}{\pi(p^2+\gamma^2)^2}S_2(p,|\mathbf{q}|),$$
$$F_2 = \frac{4M_N\gamma p}{\pi(p^2+\gamma^2)^2}S_3(p,|\mathbf{q}|),$$
$$F_3^{\mathrm{LO}} = \frac{1}{\pi}\mathrm{Im}[B_0(p,|\mathbf{q}|)^2 A_{-1}^{(^3S_1)}(p)], \tag{31}$$
$$F_4^{\mathrm{LO}} = F_3^{\mathrm{LO}}(^3S_1 \to {}^1S_0).$$

The magnitude of the relative momentum between the final-state nucleons is $2p$, with

$$p = \sqrt{M_N\nu - \gamma^2 - \frac{\mathbf{q}^2}{4} + i\epsilon}, \tag{32}$$

where $\epsilon = 0^+$. For the NC process,

$$S_2(p,|\mathbf{q}|) = 1 + \frac{\mathbf{q}^2(p^2-\gamma^2)}{2(p^2+\gamma^2)^2},$$
$$S_3(p,|\mathbf{q}|) = 1 - \frac{\mathbf{q}^2(p^2+3\gamma^2)}{6(p^2+\gamma^2)^2}, \tag{33}$$
$$B_0(p,|\mathbf{q}|) = -\sqrt{\frac{\gamma}{2\pi}}\frac{M_N}{\gamma - ip}\left(1 - \frac{\mathbf{q}^2}{12(\gamma-ip)^2}\right).$$

Note that we have further expanded the $\mathbf{q}^2$ dependence in powers of $\mathbf{q}^2/(p^2+\gamma^2)$ in order to later obtain analytic results for the Coulomb contribution in the pp channel. The error introduced is numerically small ($\ll 1\%$ in total cross section) even though the neglected terms are formally LO.

The NN scattering amplitude has an expansion

$$A = A_{-1} + A_0 + A_1 + \cdots, \tag{34}$$

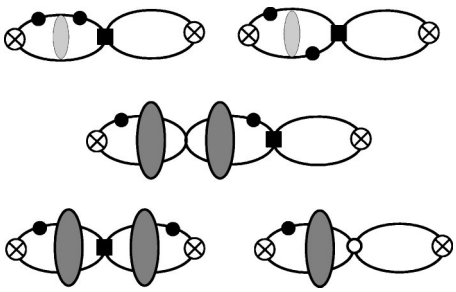

FIG. 2. Diagrams at NLO that contribute to W_0 and W_1. The black square represents an insertion of the C_2 operator in the ${}^1S_0$ channel, and $C_{2,-2}, C_{0,0}$ in the ${}^3S_1$ channel. The white circle represents an insertion of the two-body currents $L_{1,A}$ and $L_{2,A}$. Other features are as described in Fig. 1.

where the subscripts denote the powers in the small expansion parameter Q:

$$A_{-1}^{({}^3S_1)}(p)=\frac{-4\pi}{M_N}\frac{1}{\gamma+ip},$$

$$A_0^{({}^3S_1)}(p)=\frac{-2\pi}{M_N}\frac{\rho_d(p^2+\gamma^2)}{(\gamma+ip)^2}, \tag{35}$$

$$A_1^{({}^3S_1)}(p)=\frac{-\pi}{M_N}\frac{\rho_d^2(p^2+\gamma^2)^2}{(\gamma+ip)^3},$$

where $\rho_d=1.764$ fm. Also,

$$A_{-1}^{({}^1S_0)}(p)=\frac{-4\pi}{M_N}\frac{1}{\frac{1}{a^{({}^1S_0)}}+ip},$$

$$A_0^{({}^1S_0)}(p)=\frac{-2\pi}{M_N}\frac{r_0^{({}^1S_0)}p^2}{\left(\frac{1}{a^{({}^1S_0)}}+ip\right)^2}, \tag{36}$$

$$A_1^{({}^1S_0)}(p)=\frac{-\pi}{M_N}\frac{r_0^{({}^1S_0)^2}p^4}{\left(\frac{1}{a^{({}^1S_0)}}+ip\right)^3},$$

where the scattering length $a^{({}^1S_0,np)}=-23.7$ fm is known to high accuracy while the effective range $r_0^{({}^1S_0,np)}=2.73$ fm has a 2% uncertainty [34]. This uncertainty is insignificant in this calculation.

B. Next-to-leading order (NLO)

At NLO, W_0 and W_1 receive contributions from diagrams in Fig. 2 while W_3 receives contributions from diagrams in Fig. 3:

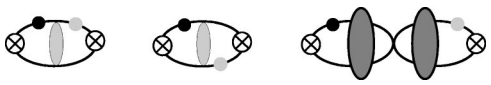

FIG. 3. Diagrams at NLO that contribute to W_3. The light gray circle represents an insertion of the nucleon magnetic moment operator. Other features are as described in Fig. 1.

$$\begin{aligned}
W_0^{\rm NLO}&=\gamma\rho_d W_0^{\rm LO}+4C_V^{(0)^2}F_3^{\rm NLO}+G_1^{\rm NLO},\\
W_1^{\rm NLO}&=\gamma\rho_d W_1^{\rm LO}+\tfrac{8}{3}C_A^{(0)^2}F_3^{\rm NLO}+\tfrac{4}{3}C_A^{(1)^2}F_4^{\rm NLO}+G_2^{\rm NLO},\\
W_3^{\rm NLO}&=-2[2(C_A^{(0)}C_M^{(0)}+C_A^{(1)}C_M^{(1)})F_1+\tfrac{1}{3}(C_A^{(0)}C_M^{(0)}\\
&\quad -C_A^{(1)}C_M^{(1)})F_2+\tfrac{8}{3}C_A^{(0)}C_M^{(0)}F_3^{\rm LO}+\tfrac{4}{3}C_A^{(1)}C_M^{(1)}F_4^{\rm LO}],
\end{aligned} \tag{37}$$

where

$$\begin{aligned}
F_3^{\rm NLO}&=F_3^{\rm LO}(A_{-1}^{({}^3S_1)}\to A_0^{({}^3S_1)}),\\
F_4^{\rm NLO}&=F_4^{\rm LO}(A_{-1}^{({}^1S_0)}\to A_0^{({}^1S_0)}),
\end{aligned} \tag{38}$$

and

$$\begin{aligned}
G_1^{\rm NLO}&=C_V^{(0)^2}\frac{2M_N\rho_d}{\pi}{\rm Im}\left[\sqrt{\frac{2\gamma}{\pi}}B_0(p,|\mathbf{q}|)A_{-1}^{({}^3S_1)}(p)\right],\\
G_2^{\rm NLO}&=-\frac{M_N}{3\pi^2}{\rm Im}\left[\sqrt{\frac{\gamma}{2\pi}}B_0(p,|\mathbf{q}|)(C_A^{(1)}\tilde{L}_{1,A}A_{-1}^{({}^1S_0)}(p)\right.\\
&\quad \left.+4C_A^{(0)}\tilde{L}_{2,A}A_{-1}^{({}^3S_1)}(p)\right).
\end{aligned} \tag{39}$$

Note that $G_1^{\rm LO}=G_2^{\rm LO}=0$. The $\tilde{L}_A$'s are renormalization scale μ-independent quantities defined as

$$\begin{aligned}
\tilde{L}_{1,A}&=-\frac{4\pi(\mu-\gamma)}{M_N C_0^{({}^1S_0)}}\\
&\quad\times\left[L_{1,A}-2\pi C_A^{(1)}\left(\frac{M_N}{2\pi}C_2^{({}^1S_0)}+\frac{\rho_d}{(\mu-\gamma)^2}\right)\right],
\end{aligned} \tag{40}$$

$$\tilde{L}_{2,A}=(\mu-\gamma)^2L_{2,A}-2\pi C_A^{(0)}\rho_d. \tag{41}$$

The expressions for $C_0^{({}^1S_0)}$ and $C_2^{({}^1S_0)}$ can be found in Appendix A. Through W_3, we become sensitive to weak magnetism at NLO, with coupling coefficients given by

$$C_M^{(0)}=-2\sin^2\vartheta_W\kappa^{(0)}-\tfrac{1}{2}\mu_S,\quad C_M^{(1)}=(1-2\sin^2\vartheta_W)\kappa^{(1)}. \tag{42}$$

C. Next-to-next-to-leading order (NNLO)

Finally, at NNLO, W_0 and W_1 receive contributions from diagrams in Figs. 4–6 while W_3 receives contributions from diagrams in Fig. 7.

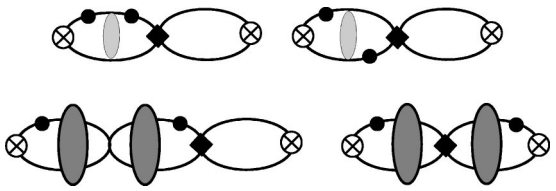

FIG. 4. Diagrams at NNLO that contribute to W_0 and W_1. The black diamond represents an insertion of the C_4 operator in the ${}^1S_0$ channel, and $C_{4,-3}$, $C_{2,-1}$, $C_{0,1}$ in the ${}^3S_1$ channel. Other features are as described in Fig. 1.

$$W_0^{\mathrm{NNLO}} = \gamma\rho_d W_0^{\mathrm{NLO}} + 4C_V^{(0)^2} F_3^{\mathrm{NNLO}} + G_1^{\mathrm{NNLO}},$$

$$W_1^{\mathrm{NNLO}} = \gamma\rho_d W_1^{\mathrm{NLO}} + \tfrac{8}{3}C_A^{(0)^2} F_3^{\mathrm{NNLO}} + \tfrac{4}{3}C_A^{(1)^2} F_4^{\mathrm{NNLO}} + G_2^{\mathrm{NNLO}}, \tag{43}$$

$$W_3^{\mathrm{NNLO}} = \gamma\rho_d W_3^{\mathrm{NLO}} - 2(\tfrac{8}{3}C_A^{(0)}C_M^{(0)} F_3^{\mathrm{NLO}} + \tfrac{4}{3}C_A^{(1)}C_M^{(1)} F_4^{\mathrm{NLO}} + G_3^{\mathrm{NLO}}),$$

where

$$F_3^{\mathrm{NNLO}} = F_3^{\mathrm{LO}}(A_{-1}^{({}^3S_1)} \to A_1^{({}^3S_1)}),$$
$$F_4^{\mathrm{NNLO}} = F_4^{\mathrm{LO}}(A_{-1}^{({}^1S_0)} \to A_1^{({}^1S_0)}), \tag{44}$$

$$G_1^{\mathrm{NNLO}} = G_1^{\mathrm{NLO}}(A_{-1}^{({}^3S_1)} \to A_0^{({}^3S_1)}) + C_V^{(0)^2}\frac{\gamma M_N^2 \rho_d^2}{2\pi^2}\mathrm{Im}[A_{-1}^{({}^3S_1)}(p)],$$

$$G_2^{\mathrm{NNLO}} = G_2^{\mathrm{NLO}}(A_{-1}^{({}^3S_1)} \to A_0^{({}^3S_1)}, A_{-1}^{({}^1S_0)} \to A_0^{({}^1S_0)}) + \frac{M_N^2\gamma}{96\pi^4}\mathrm{Im}[(\tilde{L}_{1,A}^2 A_{-1}^{({}^1S_0)}(p) + 8\tilde{L}_{2,A}^2 A_{-1}^{({}^3S_1)}(p))], \tag{45}$$

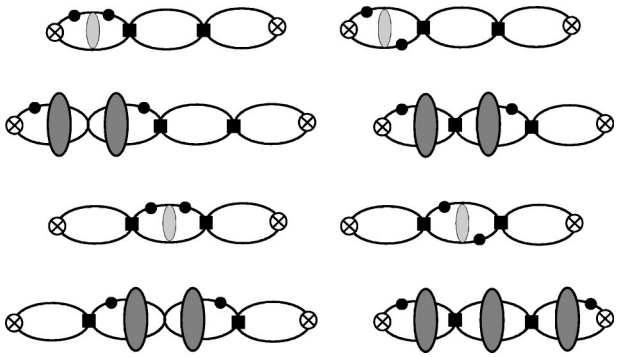

FIG. 5. Diagrams at NNLO that contribute to W_0 and W_1 through two insertions (black squares) of the C_2 operator in the ${}^1S_0$ channel, and $C_{2,-2}$, $C_{1,0}$ in the ${}^3S_1$ channel. Other features are as described in Fig. 1.

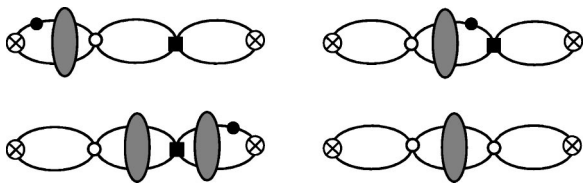

FIG. 6. Diagrams at NNLO that contribute to W_0 and W_1 through mixed insertions of the $L_{1,A}$ and $L_{2,A}$ operators (white circles) and C_2 operators (black squares). Other features are as described in Fig. 1.

$$G_3^{\mathrm{NLO}} = -\frac{M_N}{6\pi^2}\mathrm{Im}\left\{\sqrt{\frac{\gamma}{2\pi}}B_0(p,|\mathbf{q}|)[(C_M^{(1)}\tilde{L}_{1,A} + C_A^{(1)}\tilde{L}_{1,M}) \times A_{-1}^{({}^1S_0)}(p) + 4(C_M^{(0)}\tilde{L}_{2,A} + C_A^{(0)}\tilde{L}_{2,M})A_{-1}^{({}^3S_1)}(p)]\right\}.$$

Note that $G_3^{\mathrm{LO}} = G_3^{\mathrm{NLO}} = 0$. The $\tilde{L}_M$'s are μ independent quantities defined as

$$\tilde{L}_{1,M} = -\frac{8\pi(\mu-\gamma)}{M_N C_0^{({}^1S_0)}}\left[(1-2\sin^2\vartheta_W)M_N L_1 - \pi C_M^{(1)}\left(\frac{M_N}{2\pi}C_2^{({}^1S_0)} + \frac{\rho_d}{(\mu-\gamma)^2}\right)\right], \tag{46}$$

$$\tilde{L}_{2,M} = -4\sin^2\vartheta_W(\mu-\gamma)^2 M_N L_2 - 2\pi C_M^{(0)}\rho_d. \tag{47}$$

At NNLO, we should mention the effects of other partial waves, beyond *S* wave. The *P*-wave *NN* rescattering does not contribute at NNLO. The *D* wave would contribute to W_4 at NNLO, but this structure function does not contribute to the cross section, so we can neglect *D*-wave initial and final states, also.

A summary of the expressions in both this and the next section, order by order, can be found in Appendix B.

IV. $\nu(\bar{\nu})$-*D* CHARGED CURRENT INELASTIC SCATTERING

For CC processes, a few inputs change from their NC values and there are effects of electron/positron mass to consider. For $\bar{\nu}d \to e^+nn$, the sign of the last term of Eq. (23) is

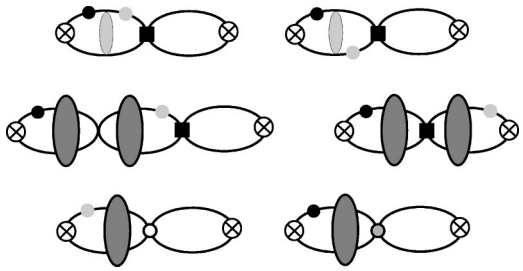

FIG. 7. Diagrams at NNLO that contribute to W_3. The filled circle represents an insertion of the two-body current L_1 or L_2. Other features are as described in Figs. 1 and 2.

TABLE I. Results for the neutral current cross sections, calculated to NNLO. The total cross section for each channel is parametrized as $\sigma(E)=a(E)+b(E)L_{1,A}$.

	$\nu_x d\to\nu_x np$ $(x=e,\mu,\tau)$		$\bar{\nu}_x d\to\bar{\nu}_x np$ $(x=e,\mu,\tau)$	
E (MeV)	a (10^{-42} cm^2)	b (10^{-42} cm^2/fm^3)	a (10^{-42} cm^2)	b (10^{-42} cm^2/fm^3)
3	0.003 15	0.000 035	0.003 12	0.000 036
4	0.0287	0.000 34	0.0282	0.000 34
5	0.0885	0.0011	0.0865	0.0011
6	0.188	0.0024	0.182	0.0024
7	0.329	0.0044	0.318	0.0043
8	0.514	0.0070	0.49	0.0069
9	0.744	0.010	0.710	0.010
10	1.02	0.015	0.968	0.014
11	1.34	0.019	1.27	0.019
12	1.72	0.025	1.61	0.025
13	2.13	0.032	1.99	0.031
14	2.60	0.039	2.41	0.038
15	3.12	0.047	2.87	0.046
16	3.69	0.056	3.37	0.054
17	4.31	0.066	3.91	0.064
18	4.97	0.077	4.49	0.074
19	5.69	0.089	5.11	0.085
20	6.47	0.102	5.76	0.097

$+$. S_1, S_2, S_3, and B_0 in Eqs. (19), (23), and (31) still take the same functional forms as for NC channels. The phase space is modified, due to the positron mass m_e and the neutron-proton mass splitting $\delta m=m_n-m_p$, to be

$$\mathrm{Max}\left[-1,-\frac{4M_N(\nu-B-\delta m)-\omega^2-\omega'^2+m_e^2}{2\omega\sqrt{\omega'^2-m_e^2}}\right]\leqslant\cos\theta\leqslant 1,$$
$$m_e\leqslant\omega'\leqslant\omega-2(M_N-\sqrt{M_N^2-M_N(B+\delta m)}). \tag{48}$$

In principle, there are also electron mass corrections to Eq. (23), but these are only important close to threshold and that region will not be probed by SNO.

For the most part, however, the primary difference between the neutral current and charged current cases is the fact that the charged current processes are purely isovector. As a result, the charged current results can be obtained from the neutral current structure factors with the substitutions:

$$\begin{aligned}
&C_V^{(0)}=0,\quad C_V^{(1)}=\frac{|V_{ud}|}{\sqrt{2}},\\
&C_A^{(0)}=0,\quad C_A^{(1)}=\frac{|V_{ud}|}{\sqrt{2}}g_A,\\
&C_M^{(0)}=0,\quad C_M^{(1)}=\sqrt{2}|V_{ud}|\kappa^{(1)},\\
&L_{1,A}\to\sqrt{2}L_{1,A}|V_{ud}|,\quad L_{2,A}=0,\\
&(1-2\sin^2\vartheta_w)L_1\to\sqrt{2}|V_{ud}|L_1,\quad L_2=0,\\
&\nu\to\nu-\delta m,
\end{aligned} \tag{49}$$

where we use $|V_{ud}|=0.975$ for this CKM matrix element. The nn scattering amplitude still has the same form as Eq. (36), as do Eqs. (40) and (46), but with different effective range parameters. We have used $a^{(^1S_0,nn)}=-18.5$ fm and $r_0^{(^1S_0,nn)}=2.80$ fm. Reference [34] indicates the uncertainty in $a^{(^1S_0,nn)}$ is at the few percent level. It is important to note that a 2% uncertainty in $a^{(^1S_0,nn)}$ will change the ν–d breakup cross section at threshold by 3–4 %.

For $\nu_e d\to e^- pp$, electromagnetic corrections in the final state are important. But instead of solving a three-body problem, we can factor out the Coulomb interaction between the electron and two protons by the Sommerfeld factor

$$S_1(|\mathbf{k}'|)=\frac{2\pi\eta_e}{1-e^{-2\pi\eta_e}}, \tag{50}$$

$$\eta_e=\frac{2\alpha\omega'}{|\mathbf{k}'|}. \tag{51}$$

This approximation is valid because the strength of a single-photon exchange between two particles with relative velocity v scales as α/v. The effect becomes sizable only when the photon exchange becomes nonperturbative, i.e., $v\leqslant\alpha$. For an electron, this velocity corresponds to a wavelength much longer than the size of the two proton system, thus Eq. (50) is justified.

For the proton-proton electromagnetic interaction, the Coulomb contribution is enhanced by a factor of $1/v$ and dominates over other short-distance photon exchange processes. We explicitly compute the long-distance Coulomb

contribution and encode the short-distance photon effects into the local operators which are then fit to the data. In this way we naturally incorporate all the isospin symmetry breaking effects in the calculation, except for the unknown counterterm $L_{1,A}$ contribution. Since the $L_{1,A}$ operator only encodes short-distance physics, the only contribution to isospin symmetry breaking is through hard photons, and thus the effect is of $\sim O(\alpha)$ and thus negligible. The other symmetry breaking effects on $L_{1,A}$ will be estimated later.

For $\nu_e d \to e^- pp$ the sign of the last term of Eq. (23) is negative $(-)$. The effects of the Coulomb interaction are encoded in the S's and B_0 as

$$S_2(p,|\mathbf{q}|)=\left(1+\frac{\mathbf{q}^2(p^2-\gamma^2-2\eta p\gamma)}{2(p^2+\gamma^2)^2}\right)\times\left(\frac{2\pi\eta}{e^{2\pi\eta}-1}\right)e^{4\eta\tan^{-1}(p/\gamma)},$$

$$S_3(p,|\mathbf{q}|)=\left(1-\frac{\mathbf{q}^2(p^2+3\gamma^2+6\eta p\gamma)}{6(p^2+\gamma^2)^2}\right)\times\left(\frac{2\pi\eta}{e^{2\pi\eta}-1}\right)e^{4\eta\tan^{-1}(p/\gamma)},\qquad(52)$$

$$\eta=\frac{\alpha M_N}{2p}.$$

$$B_0(p,|\mathbf{q}|)=M_N\int\frac{d^3k}{(2\pi)^3}\frac{\sqrt{8\pi\gamma}}{k^2+\gamma^2}\frac{2\pi\eta_k}{e^{2\pi\eta_k}-1}\frac{e^{2\eta_k\tan^{-1}(k/\gamma)}}{p^2-k^2+i\epsilon}\times\left[1+\frac{\mathbf{q}^2((1-2\eta_k^2)k^2-6\eta_k k\gamma-3\gamma^2)}{12(q^2+\gamma^2)^2}\right],\qquad(53)$$

$$\eta_k=\frac{\alpha M_N}{2k}.$$

Finally, for the pp channel, Eq. (36) must be replaced by (see Appendix A)

$$A_{-1}^{(^1S_0,pp)}(p)=\frac{-4\pi}{M_N}\frac{1}{\frac{1}{a^{(^1S_0,pp)}}+\alpha M_N H(\eta)},$$

$$A_0^{(^1S_0,pp)}(p)=\frac{-2\pi}{M_N}\frac{r_0^{(^1S_0,pp)}p^2}{\left(\frac{1}{a^{(^1S_0,pp)}}+\alpha M_N H(\eta)\right)^2},\qquad(54)$$

$$A_1^{(^1S_0,pp)}(p)=\frac{-\pi}{M_N}\frac{r_0^{(^1S_0,pp)^2}p^4}{\left(\frac{1}{a^{(^1S_0,pp)}}+\alpha M_N H(\eta)\right)^3},$$

where

$$H(\eta)=\psi(i\eta)+\frac{1}{2i\eta}-\ln(i\eta)\qquad(55)$$

with ψ the logarithmic derivative of the Γ function. Note that $A^{(^1S_0,pp)}$ in Eq. (54) is *not* the full pp scattering amplitude. It is the pp scattering amplitude with the pure Coulomb phase shift removed, as discussed in Appendix A. We have used $a^{(^1S_0,pp)}=-7.82$ fm and $r_0^{(^1S_0,pp)}=2.79$ fm. These are known to high accuracy. Furthermore, the values for $C_0^{(^1S_0)}$ and $C_2^{(^1S_0)}$ used in Eqs. (40) and (46) should be replaced by $C_{0,-1}^{(^1S_0,pp)}$ and $C_{2,-2}^{(^1S_0,pp)}$ as discussed in Appendix A.

Finally, modifications to the phase space and parameters in Eqs. (48) and (49) correspond to simply changing the sign of δm,

$$\delta m \to -\delta m.\qquad(56)$$

We note again that the expressions from this section, and the previous one, are summarized in Appendix B.

V. RESULTS

A. Unknown parameters

As discussed extensively in Ref. [13], contributions from Δs, μ_s, and $L_{2,A}$ which are not well constrained are, in fact, negligible ($\ll 1\%$) due to quasiorthogonality between initial and final states in the $^3S_1$ channel. Thus, up to NNLO the axial two-body counter term $L_{1,A}$ is the only unknown parameter contributing to each breakup channel. To estimate the effect of isospin-symmetry breaking on $L_{1,A}$, we consider how much $L_{1,A}$ must vary in order for $\tilde{L}_{1,A}$ [defined in Eq. (40)] to take on a universal value. This assumes that the symmetry breaking effects in $C_0^{(^1S_0)}$, $C_2^{(^1S_0)}$, and $L_{1,A}$ are all comparable. The effect is $\sim 10\%$ in the value of $L_{1,A}$ at $\mu=m_\pi$ for a natural value of $L_{1,A}$ given by dimensional analysis

$$|L_{1,A}|\approx\frac{1}{M_\pi}\frac{1}{(m_\pi-\gamma)^2}\approx 6\ \text{fm}^3.\qquad(57)$$

This 10% uncertainty in $L_{1,A}$ corresponds to a 1% uncertainty in the total cross sections. This means that we can treat the symmetry breaking effect on $L_{1,A}$ as higher order, and that we can take $L_{1,A}$ to be the same in all four channels to the precision of this calculation.

B. Total cross sections

We are now able to present a systematic and convergent picture of inelastic neutrino-deuteron scattering in all four channels: neutral current $\nu_x(\bar{\nu}_x)d\to\nu_x(\bar{\nu}_x)pn$ (NC) with $x=e,\mu,\tau$, and charged current $\nu_e d\to e^- pp$ and $\bar{\nu}_e d\to e^+ nn$ (CC).

We parametrize the cross sections as

$$\sigma(E)=a(E)+b(E)L_{1,A},$$

TABLE II. Results for the charged current cross sections calculated to NNLO. The total cross section for each channel is parametrized as $\sigma(E)=a(E)+b(E)L_{1,A}$.

	$\nu_e d\to e^- pp$		$\bar{\nu}_e d\to e^+ nn$	
E (MeV)	a (10^{-42} cm^2)	b (10^{-42} cm^2/fm^3)	a (10^{-42} cm^2)	b (10^{-42} cm^2/fm^3)
2	0.003 44	0.000 031		
3	0.0439	0.000 44		
4	0.146	0.0016		
5	0.320	0.0036	0.0264	0.000 30
6	0.574	0.0067	0.110	0.0014
7	0.914	0.011	0.261	0.0034
8	1.34	0.017	0.482	0.0065
9	1.87	0.024	0.776	0.011
10	2.48	0.032	1.14	0.016
11	3.20	0.042	1.58	0.023
12	4.01	0.054	2.09	0.032
13	4.93	0.067	2.68	0.041
14	5.95	0.082	3.33	0.052
15	7.08	0.098	4.06	0.065
16	8.31	0.12	4.85	0.079
17	9.66	0.14	5.71	0.094
18	11.12	0.16	6.63	0.11
19	12.70	0.18	7.63	0.13
20	14.39	0.21	8.68	0.15

where the coupling constant of the axial two-body current $L_{1,A}$ (with $\mu=m_\pi$) is given in units of fm^3, and present the results in Tables I and II. There are also terms quadratic in $L_{1,A}$ at NNLO, but they are not significant for values of $L_{1,A}$ considered here. We will neglect these quadratic terms.

We have performed this calculation to NNLO largely to test the convergence of the calculation and, in turn, be able to place constraints on the theoretical uncertainties in the calculation of $\nu(\bar{\nu})-d$ breakup. In Fig. 8 we compare the size of NLO and NNLO contributions to the cross sections against the LO contribution. Given the uncertainty in $L_{1,A}$, we consider values -5 fm$^3\leqslant L_{1,A}\leqslant 5$ fm^3. The shaded areas represent the range of NLO and NNLO contributions possible for these values of $L_{1,A}$. We see that the typical NLO contribution is of order 5–20 %, while the typical NNLO contribution is less than 5% and, better still, less than 3% above 5 MeV.

A clearer picture of convergence emerges if we decompose the cross sections into a symmetric piece arising from structure factors receiving contributions at all three orders (W_1 and W_2), and an antisymmetric piece receiving contributions only at NLO and NNLO (W_3). This is done for the neutral current cross sections in Fig. 9, where we see a cleaner separation between size of the NLO and NNLO contributions. From this we can expect, with some confidence, that the NNNLO contribution will be less than 3%. This in turn represents the formal theoretical uncertainty in our calculation.

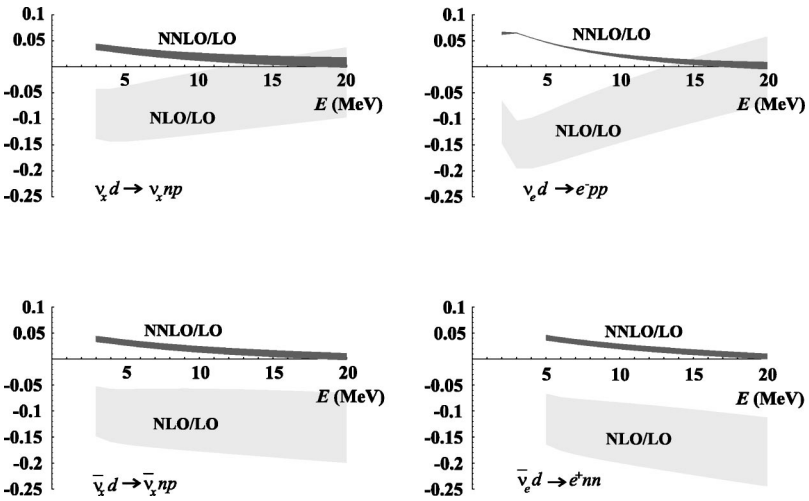

FIG. 8. Testing convergence of the EFT calculation in each of the four channels studied. Shown are the relative NLO and NNLO contributions to the total cross section in each channel, for values of $L_{1,A}$ between -5 fm^3 and $+5$ fm^3. Note that $\nu_x(\bar{\nu}_x)$ represents e, μ, or τ neutrinos (antineutrinos).

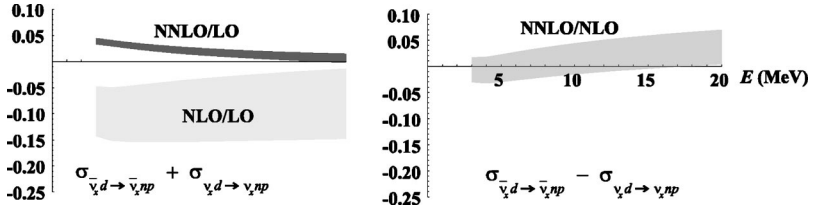

FIG. 9. A further test of the convergence of the EFT calculation, using the NC channel. The left-hand graph arises from comparing contributions from the sum of the νd and $\bar{\nu}d$ channels, or specifically the contributions from W_1 and W_2 which received contributions from all three orders of perturbation theory. The right-hand graph looks at the difference between the two channels, or specifically the contributions from W_3 which appear at NLO and NNLO only. As in Fig 8, the shaded areas represent the effect of varying $L_{1,A}$ between -5 fm^3 and $+5$ fm^3.

We compare our results to those of the potential model calculations NSGK [12] and YHH [11] in Fig. 10. We perform a global fit of our results to these model calculations with $L_{1,A}$ as the only free parameter. We find that the best fit to NSGK is given by $L_{1,A}^{\mathrm{NSGK}}=5.6$ fm^3, and for YHH $L_{1,A}^{\mathrm{YHH}}=0.94$ fm^3. These values are both consistent with the natural value of $L_{1,A}$ estimated in Eq. (57) and the quality of the fit is impressive. This indicates the 5–10 % difference in two potential model calculations is largely due to different assumptions made about short distance physics.

We further examine the ratios of our cross sections to the potential model results of NSGK and YHH in Figs. 11 and 12, respectively. We see that there are deviations of order 5% between our result and YHH in all four channels. The fluctuations seen are in the results of YHH, and disagreements at threshold are most likely due to differences in the effective range parameters that can be associated with each calculation. However, the agreement between our result at NSGK is quite impressive—better than 1% over the whole range of neutrino energies studied. For comparison, we note the effective range parameters used here and those calculated from the potential used in NSGK [35] (using the Argonne v_{18} potential [36], but with only Coulomb electromagnetic interactions) in Table III.

Of importance to SNO is the ratio between charged and neutral current cross sections

$$R \equiv \frac{\sigma_{\mathrm{CC}}}{\sigma_{\mathrm{NC}}}. \tag{58}$$

As shown in Ref. [13], this ratio R at NLO was insensitive to the value of $L_{1,A}$, and that is still true at NNLO as seen in Fig. 13. We consider two ratios, for both the $\nu-d$ (relevant to SNO) and $\bar{\nu}-d$ channels. The latter was the only channel discussed in Ref. [13]. Variations of $L_{1,A}$ over a large range, from -20 to $+40$ fm^3, leads to a 6% variation in R. This likely represents an extreme variation, as it leads to as much as a 90% change in the total cross sections. The actual uncertainty in R is almost certainly much less. Further, we can see that our values of R agree well with the potential model

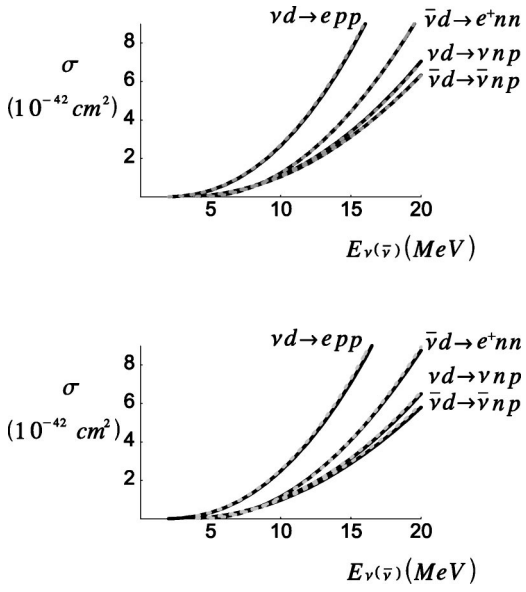

FIG. 10. Inelastic $\nu(\bar{\nu})d$ cross sections as a function of incident $\nu(\bar{\nu})$ energy. The solid curves in the upper graph are NSGK [12], while the dashed curves are the EFT results at NNLO, fit with $L_{1,A}=5.6$ fm^3. The solid curves in the lower graph are the results of YHH [11], and the dashed curves are the NNLO EFT results fit with $L_{1,A}=0.94$ fm^3. In both graphs, the dashed curves all lie right on top of the solid curves.

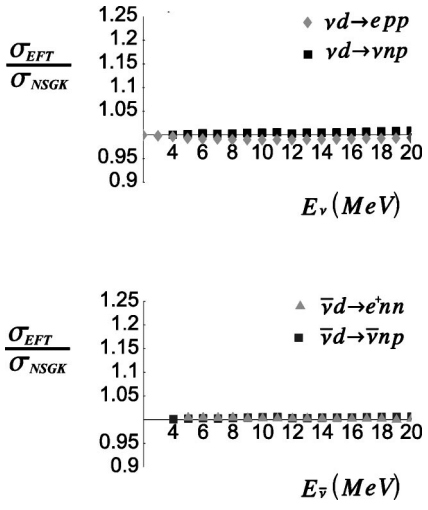

FIG. 11. Ratios between the EFT calculation at NNLO and the potential model result of NSGK [12]. The upper graph compares the two channels of $\nu-d$ scattering, and the lower graph the two channels of $\bar{\nu}-d$ scattering. Agreement is better than 1% over the whole range of energies shown, for a single value of $L_{1,A}=5.6$ fm^3.

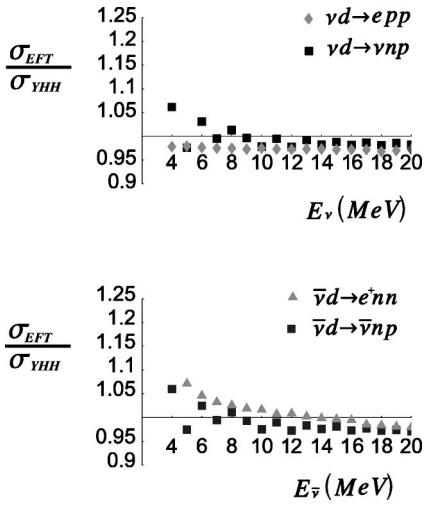

FIG. 12. As in Fig. 11, but comparing to the potential model result of YHH [11]. The agreement is not as good here, using a best-fit value of $L_{1,A}=0.94$ fm^3.

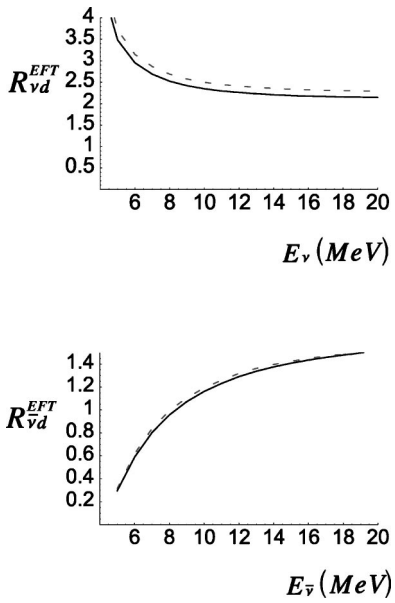

FIG. 13. CC to NC cross-section ratios for $\nu-d$ and $\bar{\nu}-d$ scattering, as functions of incident energy. Shown are ratios of the EFT NNLO results with $L_{1,A}=-20$ fm^3 (dashed curves) and $L_{1,A}=40$ fm^3 (solid curves), demonstrating the insensitivity of the ratio to the value of $L_{1,A}$.

results (Fig. 14), with the worst agreement being seen when comparing to YHH. We use a median value of $L_{1,A}=3.7$ fm^3 for this comparison. The poor agreement with YHH is biased towards threshold, and the likely reasons for this have already been discussed.

VI. SUMMARY AND CONCLUSIONS

We have performed a calculation to NNLO of all four channels of νd and $\bar{\nu} d$ breakup. Our work agrees very well with the latest potential model calculations, subject to the fitting of a single unknown counterterm $L_{1,A}$. Working at NNLO has allowed us to determine that our calculation indeed converges at the neutrino energies of interest, which in turn allows us to determine a formal theoretical uncertainty of 3% in our calculation. The only outstanding issue continues to be the determination of $L_{1,A}$.

It is imperative that an experimental determination of this counterterm be made. The theory without pions cannot reach energies that would allow this to be done with sample, but a breakthrough in the treatment of pions at NNLO might make access possible in the full theory. For now, ORLaND offers the best hope, with plans for a high-precision measurement in the $\nu-d$ CC channel.

ACKNOWLEDGMENTS

We would like to thank Martin Savage, Tom Cohen, John Beacom, and Hamish Robertson for useful discussions. We would like to thank K. Kubodera for providing us with the results of a new potential model calculation (NSGK) and T. Sato for providing information on that calculation's effective range parameters. We thank the Department of Physics at the University of Washington where this work was initiated, the Institute for Nuclear Theory at the University of Washington for its hospitality, and the U.S. Department of Energy for partial support during the completion of this work. J.-W.C. is supported, in part, by the Department of Energy under Grant No. DOE/ER/40762-213. M.B. and X.K. are supported by grants from the Natural Sciences and Engineering Research Council of Canada.

APPENDIX A: FITTING THE PARAMETERS OF EFFECTIVE FIELD THEORY

Here, we summarize the fits to parameters in the theory without pions.

1. The $^3S_1$ channel

In the $^3S_1$ channel, we use the effective range expansion about the deuteron pole. Thus,

$$p \cot \delta_0 = -\gamma + \tfrac{1}{2}\rho_d(p^2+\gamma^2) + \cdots . \qquad \text{(A1)}$$

TABLE III. Effective range parameters as used in our work and NSGK [12].

	$a^{^1S_0,pp}$ (fm)	$r_0^{^1S_0,pp}$ (fm)	$a^{^1S_0,nn}$ (fm)	$r_0^{^1S_0,nn}$ (fm)	$a^{^1S_0,np}$ (fm)	$r_0^{^1S_0,np}$ (fm)	ρ_d (fm)
This work	−7.82	2.79	−18.5	2.80	−23.7	2.73	1.764
NSGK	−7.815	2.78	−18.5	2.83	−23.73	2.69	1.767

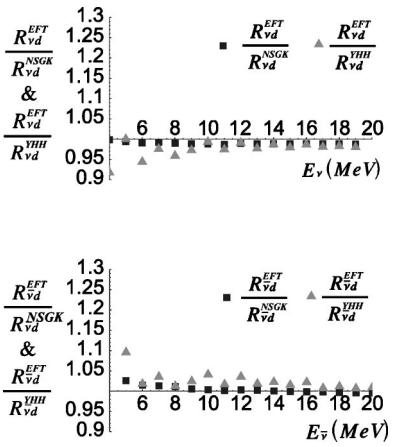

FIG. 14. The ''ratio of ratios'' between the EFT results at NNLO and those of NSGK [12] and YHH [11], with the EFT results using a median value of $L_{1,A}=3.7$ fm^3. The upper graph compares the ratios for $\nu-d$ scattering, and the lower graph the ratios for $\bar{\nu}-d$ scattering. Again, the agreement with NSGK is excellent.

To keep the deuteron pole position unchanged at each order in perturbation theory, we expand

$$C_0^{(^3S_1)}=C_{0,-1}^{(^3S_1)}+C_{0,0}^{(^3S_1)}+C_{0,1}^{(^3S_1)}+\cdots,$$

$$C_2^{(^3S_1)}=C_{2,-2}^{(^3S_1)}+C_{2,-1}^{(^3S_1)}+\cdots, \tag{A2}$$

$$C_4^{(^3S_1)}=C_{4,-3}^{(^3S_1)}+\cdots,$$

where the first index continues to denote the momentum dependence while the second index indicates the explicit power counting in the Q expansion. Using the definition of the scattering amplitude

$$\mathcal{A}=\frac{4\pi}{M_N}\frac{1}{p\cot\delta_0-ip} \tag{A3}$$

along with the amplitude computed using the power divergent subtraction (PDS) scheme proposed by KSW [14]

$$\mathcal{A}_{EFE}=-\frac{1}{\frac{1}{C}+\frac{M_N}{4\pi}(\mu+ip)} \tag{A4}$$

with $C=\Sigma C_{2n}^{(^3S_1)}p^{2n}$.

Matching terms order by order in a Q expansion, one obtains

$$C_{0,-1}^{(^3S_1)}=\frac{-4\pi}{M_N}\frac{1}{(\mu-\gamma)},$$

$$C_{0,0}^{(^3S_1)}=\frac{2\pi}{M_N}\frac{\rho_d\gamma^2}{(\mu-\gamma)^2},$$

$$C_{0,1}^{(^3S_1)}=-\frac{\pi}{M_N}\frac{\rho_d^2\gamma^4}{(\mu-\gamma)^3},$$

$$C_{2,-2}^{(^3S_1)}=\frac{2\pi}{M_N}\frac{\rho_d}{(\mu-\gamma)^2}, \tag{A5}$$

$$C_{2,-1}^{(^3S_1)}=-\frac{2\pi}{M_N}\frac{\rho_d^2\gamma^2}{(\mu-\gamma)^3},$$

$$C_{4,-3}^{(^3S_1)}=-\frac{\pi}{M_N}\frac{\rho_d^2}{(\mu-\gamma)^3},$$

where we have neglected relativistic corrections.

2. The $^1S_0$ channel

We will deal with the pp channel separately in the next section. For the np and nn channels, the procedure is somewhat simpler. The effective range expansion is given by

$$p\cot\delta_0=-\frac{1}{a}+\frac{1}{2}r_0p^2+\cdots. \tag{A6}$$

Here, one obtains

$$C_0^{(^1S_0)}=\frac{-4\pi}{M_N}\frac{1}{\left(\mu-\frac{1}{a^{(^1S_0)}}\right)},$$

$$C_2^{(^1S_0)}=\frac{2\pi}{M_N}\frac{r_0^{(^1S_0)}}{\left(\mu-\frac{1}{a^{(^1S_0)}}\right)^2}, \tag{A7}$$

$$C_4^{(^1S_0)}=-\frac{\pi}{M_N}\frac{r_0^{(^1S_0)^2}}{\left(mu-\frac{1}{a^{(^1S_0)}}\right)^3}.$$

3. The $^1S_0$ pp channel

In this section we show how we fix the pp scattering parameters to phase shift data through matching on to effective range expansion.

The S-wave pp scattering amplitude can be decomposed into

$$\mathcal{A}=\mathcal{A}_C+\mathcal{A}_{SC}, \tag{A8}$$

where $\mathcal{A}_C$ is the pure Coulomb interaction amplitude with strong interaction ''turned off'' and $\mathcal{A}_{SC}$ is the remaining part with both strong and Coulomb interactions. Phase shifts δ and δ_C are defined by

$$\mathcal{A}=\frac{4\pi}{M_N}\frac{e^{2i\delta}-1}{2ip},$$
$$\mathcal{A}_C=\frac{4\pi}{M_N}\frac{e^{2i\delta_C}-1}{2ip}. \tag{A9}$$

Then

$$\mathcal{A}_{SC}=\frac{4\pi}{M_N}e^{2i\delta_C}\left(\frac{e^{2i\delta_{SC}}-1}{2ip}\right)=\frac{4\pi}{M_N}\frac{e^{2i\delta_C}}{p(\cot\delta_{SC}-i)}, \tag{A10}$$

where $\delta_{SC}\equiv\delta-\delta_C$. The effective range expansion states that

$$p(\cot\delta_{SC}-i)=\left(-\frac{1}{a^{(pp)}}+\frac{1}{2}r_0^{(pp)}p^2+v^{(pp)}p^4+\cdots\right)-\alpha M_N H(\eta), \tag{A11}$$

where $v^{(pp)}$ is the shape parameter. This expansion is related to $\mathcal{A}_{SC}/e^{2i\delta_C}$ which can be thought of as the pp scattering amplitude with the pure Coulomb phase shift removed. The sum of the diagrams gives

$$\frac{\mathcal{A}_{SC}}{e^{2i\delta_C}}\equiv A^{(^1S_0,pp)}=-\frac{1}{\frac{1}{C}-J_0}, \tag{A12}$$

where

$$C=\sum_{n=0}^{\infty}C_{2n}^{(pp)}(p^2-\alpha M_N\mu)^n \tag{A13}$$

and

$$J_0=\frac{\alpha M_N^2}{4\pi}\left(\ln\frac{\mu\sqrt{\pi}}{\alpha M_N}+1-\frac{3}{2}\gamma_E\right)-\frac{\mu M_N}{4\pi}-\frac{\alpha M_N^2}{4\pi}H(\eta) \tag{A14}$$

with the Euler's constant $\gamma_E=0.577$. In Eq. (A14), a four-dimensional pole $\alpha M_N^2/(4\pi(4-d))$, along with the three-dimensional pole, are subtracted from J_0 using the PDS prescription.

It is convenient to insert the expansion parameter ε into Eqs. (A10)–(A12) to keep track of the Q expansion. Then the effective field theory parameters $C_{2n}^{(pp)}$ can be solved by matching the effective range expansion order by order in ε. The insertion of ε is done by the transformation

$$\frac{1}{a^{(pp)}}\to\frac{1}{a^{(pp)}}\varepsilon,\quad p\to p\varepsilon,$$
$$r_0^{(pp)}\to r_0^{(pp)},\quad v^{(pp)}\to v^{(pp)},$$
$$\alpha M_N\to\alpha M_N\varepsilon,\quad \mu\to\mu\varepsilon,$$
$$H(\eta)\to H(\eta),\quad J_0\to J_0\varepsilon. \tag{A15}$$

The assignment of powers in ε reflects the powers in Q scaling of those parameters. For example, $1/a^{(pp)}$ and p scale like Q, αM_N scales like Q^2 while $|H(\eta)|\leqslant p/(\alpha M_N)$ scales like ε^0. The $C_{2n}^{(pp)}$ can be represented in a manner analogous to that shown in the $^3S_1$ channel [19]

$$C_0^{(pp)}=C_{0,-1}^{(pp)}\varepsilon^{-1}+C_{0,0}^{(pp)}+C_{0,1}^{(pp)}\varepsilon+\cdots,$$
$$C_2^{(pp)}=C_{2,-2}^{(pp)}\varepsilon^{-2}+C_{2,-1}^{(pp)}\varepsilon^{-1}+\cdots, \tag{A16}$$
$$C_4^{(pp)}=C_{4,-3}^{(pp)}\varepsilon^{-3}+\cdots.$$

Then from Eqs. (A10)–(A12) we obtain

$$C_{0,-1}^{(pp)}=\frac{4\pi}{M_N}\frac{1}{\frac{1}{a^{(pp)}}-\mu+\alpha M_N\left(\ln\frac{\mu\sqrt{\pi}}{\alpha M_N}+1-\frac{3}{2}\gamma_E\right)} \tag{A17}$$

and

$$C_{0,0}^{(pp)}=\frac{\alpha M_N^2\mu\gamma_0{}^{(pp)}}{8\pi}C_{0,-1}^{(pp)^2},$$
$$C_{0,1}^{(pp)}=\frac{\alpha^2M_N^4\mu^2\gamma_0{}^{(pp)^2}}{64\pi^2}C_{0,-1}^{(pp)^3},\quad C_{2,-2}^{(pp)}=\frac{M_N}{8\pi}r_0^{(pp)}C_{0,-1}^{(pp)^2},$$
$$C_{2,-1}^{(pp)}=\frac{\alpha M_N^3\mu\gamma_0^{(pp)^2}}{32\pi^2}C_{0,-1}^{(pp)^3},\quad C_{4,-3}^{(pp)}=\frac{M_N^2}{64\pi^2}r_0^{(pp)^2}C_{0,-1}^{(pp)^3}. \tag{A18}$$

The solutions of parameters for nn and $np^{(^1S_0)}$ given in the preceding section can be obtained by taking $\alpha=0$ from the above expressions.

APPENDIX B: SUMMARY OF SCATTERING CROSS SECTION

In this appendix, we explicitly list the relevant formulas for the four $\nu(\bar{\nu})d$ breakup processes. To make the formulas compact, certain higher order terms have been resummed. The Q-expansion expressions to NNLO shown in the text can always be recovered by expanding in ϵ to $\mathcal{O}(\epsilon^2)$. Here ϵ is just a device to keep track of the Q expansion—its value should be set to 1 after the expansion is performed.

1. $\nu+d\to\nu+n+p$ and $\bar{\nu}+d\to\nu+n+p$

Differential cross section

$$\frac{d^2\sigma}{d\omega'\,d\Omega}=\frac{G_F^2\omega'|\mathbf{k}'|}{2\pi^2}\left[2W_1\sin^2\frac{\theta}{2}+W_2\cos^2\frac{\theta}{2}\mp 2\frac{(\omega+\omega')}{M_d}W_3\sin^2\frac{\theta}{2}\right], \tag{B1}$$

with $-(+)$ sign for the $\nu(\bar{\nu})d$ scattering.

Phase space

$$\mathrm{Max}\left[-1,1-\frac{4M_N(\nu-B)-\nu^2}{2\omega\omega'}\right]\leqslant\cos\theta\leqslant 1,$$
$$0\leqslant\omega'\leqslant\omega-2(M_N-\sqrt{M_N^2-\gamma^2}). \tag{B2}$$

Structure functions [as mentioned above, one can obtain the NNLO results by expanding ϵ to $\mathcal{O}(\epsilon^2)$]

$$W_1=\frac{1}{(1-\epsilon\gamma\rho_d)}\left[2(C_A^{(0)^2}+C_A^{(1)^2})F_1+\frac{1}{3}(C_A^{(0)^2}-C_A^{(1)^2})F_2+\frac{8}{3}C_A^{(0)^2}F_3+\frac{4}{3}C_A^{(1)^2}F_4+G_2\right],$$

$$W_2=W_1+\frac{1}{(1-\epsilon\gamma\rho_d)}[2(C_V^{(0)^2}+C_V^{(1)^2})F_1+(C_V^{(0)^2}-C_V^{(1)^2})\times F_2+4C_V^{(0)^2}F_3+G_1], \tag{B3}$$

$$W_3=\frac{-2\epsilon}{(1-\epsilon\gamma\rho_d)}\left[2(C_A^{(0)}C_M^{(0)}+C_A^{(1)}C_M^{(1)})F_1+\frac{1}{3}(C_A^{(0)}C_M^{(0)}-C_A^{(1)}C_M^{(1)})F_2+\frac{8}{3}C_A^{(0)}C_M^{(0)}F_3+\frac{4}{3}C_A^{(1)}C_M^{(1)}F_4+G_3\right],$$

$$C_V^{(0)}=-\sin^2\vartheta_W,\quad C_V^{(1)}=\tfrac{1}{2}(1-2\sin^2\vartheta_W),$$
$$C_A^{(0)}=-\tfrac{1}{2}\Delta s,\quad C_A^{(1)}=\tfrac{1}{2}g_A, \tag{B4}$$

$$C_M^{(0)}=-2\sin^2\vartheta_W\kappa^{(0)}-\tfrac{1}{2}\mu_S,\quad C_M^{(1)}=(1-2\sin^2\vartheta_W)\kappa^{(1)}.$$

$$F_1=\frac{2M_N\gamma p}{\pi(p^2+\gamma^2)^2}\left(1+\frac{\mathbf{q}^2(p^2-\gamma^2)}{2(p^2+\gamma^2)^2}\right),$$

$$F_2=\frac{4M_N\gamma p}{\pi(p^2+\gamma^2)^2}\left(1-\frac{\mathbf{q}^2(p^2+3\gamma^2)}{6(p^2+\gamma^2)^2}\right), \tag{B5}$$

$$F_3=\frac{1}{\pi}\mathrm{Im}[{B_0}^2(A_{-1}^{(^3S_1)}(p)+\epsilon A_0^{(^3S_1)}(p)+\epsilon^2A_1^{(^3S_1)}(p))],$$

$$F_4=F_3(^3S_1\rightarrow{}^1S_0,np),$$

$$B_0=-\sqrt{\frac{\gamma}{2\pi}}\frac{M_N}{\gamma-ip}\left(1-\frac{\mathbf{q}^2}{12(\gamma-ip)^2}\right), \tag{B6}$$

$$p=\sqrt{M_N\nu-\gamma^2-\frac{\mathbf{q}^2}{4}+i\epsilon}, \tag{B7}$$

$$G_1=\epsilon{C_V^{(0)}}^2\frac{2M_N\rho_d}{\pi}\mathrm{Im}\left[\sqrt{\frac{2\gamma}{\pi}}B_0(A_{-1}^{(^3S_1)}(p)+\epsilon A_0^{(^3S_1)}(p))\right],$$

$$G_2=-\epsilon\frac{M_N}{3\pi^2}\mathrm{Im}\left[\sqrt{\frac{\gamma}{2\pi}}B_0[C_A^{(1)}\tilde{L}_{1,A}(A_{-1}^{(^1S_0,np)}(p)+\epsilon A_0^{(^1S_0,np)}(p))+4C_A^{(0)}\tilde{L}_{2,A}(A_{-1}^{(^3S_1)}(p)+\epsilon A_0^{(^3S_1)}(p))]\right]+\epsilon^2\frac{M_N^2\gamma}{96\pi^4}\mathrm{Im}[(\tilde{L}_{1,A}^2A_{-1}^{(^1S_0,np)}(p)+8\tilde{L}_{2,A}^2A_{-1}^{(^3S_1)}(p))], \tag{B8}$$

$$G_3=\epsilon^2\frac{M_N}{3\pi^2}\mathrm{Im}\left\{\sqrt{\frac{\gamma}{2\pi}}B_0(p,|\mathbf{q}|)[(C_M^{(1)}\tilde{L}_{1,A}+C_A^{(1)}\tilde{L}_{1,M})\times A_{-1}^{(^1S_0,np)}(p)+4(C_M^{(0)}\tilde{L}_{2,A}+C_A^{(0)}\tilde{L}_{2,M})A_{-1}^{(^3S_1)}(p)]\right\},$$

$$\tilde{L}_{1,A}=-\frac{4\pi(\mu-\gamma)}{M_NC_0^{(^1S_0,np)}}\left[L_{1,A}-2\pi C_A^{(1)}\times\left(\frac{M_N}{2\pi}C_2^{(^1S_0,np)}+\frac{\rho_d}{(\mu-\gamma)^2}\right)\right], \tag{B9}$$

$$\tilde{L}_{2,A}=(\mu-\gamma)^2L_{2,A}-2\pi C_A^{(0)}\rho_d.$$

$$\tilde{L}_{1,M}=-\frac{8\pi(\mu-\gamma)}{M_NC_0^{(^1S_0,np)}}\left[(1-2\sin^2\vartheta_W)M_NL_1-\pi C_M^{(1)}\left(\frac{M_N}{2\pi}C_2^{(^1S_0,np)}+\frac{\rho_d}{(\mu-\gamma)^2}\right)\right], \tag{B10}$$

$$\tilde{L}_{2,M}=-4\sin^2\vartheta_W(\mu-\gamma)^2M_NL_2-2\pi C_M^{(0)}\rho_d,$$

evaluated at $\mu=m_\pi$, with $C_0^{(^1S_0,np)}=-3.56$ fm^2 and $C_2^{(^1S_0,np)}=6.55$ fm^4. Further, $\Delta s=-0.17$ and $\mu_s=L_{2,A}=0$ are used in our calculation (though the results are not sensitive to these choices).

2. $\bar{\nu}+d\rightarrow e^++n+n$

Differential cross section

$$\frac{d^2\sigma}{d\omega'\,d\Omega}=\frac{G_F^2\omega'|\mathbf{k}'|}{2\pi^2}\left[2W_1\sin^2\frac{\theta}{2}+W_2\cos^2\frac{\theta}{2}+2\frac{(\omega+\omega')}{M_d}W_3\sin^2\frac{\theta}{2}\right], \tag{B11}$$

Phase space

$$\mathrm{Max}\left[-1,-\frac{4M_N(\nu-B+m_n-m_p)-\omega^2-\omega'^2+m_e^2}{2\omega\sqrt{\omega'^2-m_e^2}}\right] \leqslant \cos\theta \leqslant 1, \tag{B12}$$

$$m_e \leqslant \omega' \leqslant \omega - 2(M_N - \sqrt{M_N^2 - M_N(B-m_n+m_p)}).$$

Structure functions

$$W_1 = \frac{1}{(1-\epsilon\gamma\rho_d)}\left[2C_A^{(1)^2}F_1 - \frac{1}{3}C_A^{(1)^2}F_2 + \frac{4}{3}C_A^{(1)^2}F_4 + G_2\right],$$

$$W_2 = W_1 + \frac{1}{(1-\epsilon\gamma\rho_d)}[2C_V^{(1)^2}F_1 - C_V^{(1)^2}F_2], \tag{B13}$$

$$W_3 = \frac{-2\epsilon}{(1-\epsilon\gamma\rho_d)}\left[2C_A^{(1)}C_M^{(1)}F_1 - \frac{1}{3}C_A^{(1)}C_M^{(1)}F_2 + \frac{4}{3}C_A^{(1)}C_M^{(1)}F_4 + G_3\right].$$

$$p = \sqrt{M_N(\nu+m_n-m_p) - \gamma^2 - \frac{\mathbf{q}^2}{4} + i\epsilon}, \tag{B14}$$

$$C_V^{(1)} = \frac{|V_{ud}|}{\sqrt{2}}, \quad C_A^{(1)} = \frac{|V_{ud}|}{\sqrt{2}}g_A, \quad C_M^{(1)} = \sqrt{2}|V_{ud}|\kappa^{(1)}, \tag{B15}$$

$$F_1 = \frac{2M_N\gamma p}{\pi(p^2+\gamma^2)^2}\left(1+\frac{\mathbf{q}^2(p^2-\gamma^2)}{2(p^2+\gamma^2)^2}\right),$$

$$F_2 = \frac{4M_N\gamma p}{\pi(p^2+\gamma^2)^2}\left(1-\frac{\mathbf{q}^2(p^2+3\gamma^2)}{6(p^2+\gamma^2)^2}\right), \tag{B16}$$

$$F_4 = \frac{1}{\pi}\mathrm{Im}[B_0{}^2(A_{-1}^{(^1S_0,nn)}(p) + \epsilon A_0^{(^1S_0,nn)}(p) + \epsilon^2 A_1^{(^1S_0,nn)}(p))],$$

$$G_2 = -\epsilon\frac{M_N}{3\pi^2}\mathrm{Im}\left[\sqrt{\frac{\gamma}{2\pi}}B_0C_A^{(1)}\tilde{L}_{1,A}(A_{-1}^{(^1S_0,nn)}(p) + \epsilon A_0^{(^1S_0,nn)}(p))\right] + \epsilon^2\frac{M_N^2\gamma}{96\pi^4}\mathrm{Im}[\tilde{L}_{1,A}^2A_{-1}^{(^1S_0,nn)}(p)], \tag{B17}$$

$$G_3 = \epsilon^2\frac{M_N}{3\pi^2}\mathrm{Im}\left[\sqrt{\frac{\gamma}{2\pi}}B_0(C_M^{(1)}\tilde{L}_{1,A} + C_A^{(1)}\tilde{L}_{1,M})A_{-1}^{(^1S_0,nn)}(p)\right].$$

$$\tilde{L}_{1,A} = -\frac{4\pi(\mu-\gamma)}{M_NC_0^{(^1S_0,nn)}}\left[\sqrt{2}|V_{ud}|L_{1,A} - 2\pi C_A^{(1)}\left(\frac{M_N}{2\pi}C_2^{(^1S_0,nn)} + \frac{\rho_d}{(\mu-\gamma)^2}\right)\right], \tag{B18}$$

$$\tilde{L}_{1,M} = -\frac{8\pi(\mu-\gamma)}{M_NC_0^{(^1S_0,nn)}}\left[\sqrt{2}|V_{ud}|M_NL_1 - \pi C_M^{(1)}\left(\frac{M_N}{2\pi}C_2^{(^1S_0,nn)} + \frac{\rho_d}{(\mu-\gamma)^2}\right)\right],$$

evaluated at $\mu = m_\pi$, with $C_0^{(^1S_0,nn)} = -3.49$ fm^2 and $C_2^{(^1S_0,nn)} = 6.46$ fm^4.

3. $\nu_e + d \to e^- + p + p$

Differential cross section

$$\frac{d^2\sigma}{d\omega'\,d\Omega} = \frac{G_F^2\omega'|\mathbf{k}'|}{2\pi^2}\frac{2\pi\eta_e}{1-e^{-2\pi\eta_e\eta_e}}\left[2W_1\sin^2\frac{\theta}{2} + W_2\cos^2\frac{\theta}{2} - 2\frac{(\omega+\omega')}{M_d}W_3\sin^2\frac{\theta}{2}\right], \tag{B19}$$

$$\eta_e = \frac{2\alpha\omega'}{|\mathbf{k}'|}.$$

Phase space

$$\mathrm{Max}\left[-1,-\frac{4M_N(\nu-B+m_n-m_p)-\omega^2-\omega'^2+m_e^2}{2\omega\sqrt{\omega'^2-m_e^2}}\right] \leqslant \cos\theta \leqslant 1, \tag{B20}$$

$$m_e \leqslant \omega' \leqslant \omega - 2(M_N - \sqrt{M_N^2 - M_N(B-m_n+m_p)}).$$

Structure functions

$$W_1 = \frac{1}{(1-\epsilon\gamma\rho_d)}\left[2C_A^{(1)^2}F_1 - \frac{1}{3}C_A^{(1)^2}F_2 + \frac{4}{3}C_A^{(1)^2}F_4 + G_2\right],$$

$$W_2 = W_1 + \frac{1}{(1-\epsilon\gamma\rho_d)}[2C_V^{(1)^2}F_1 - C_V^{(1)^2}F_2], \tag{B21}$$

$$W_3 = \frac{-2\epsilon}{(1-\epsilon\gamma\rho_d)}\left[2C_A^{(1)}C_M^{(1)}F_1 - \frac{1}{3}C_A^{(1)}C_M^{(1)}F_2 + \frac{4}{3}C_A^{(1)}C_M^{(1)}F_4 + G_3\right],$$

$$F_1=\frac{2M_N\gamma p}{\pi(p^2+\gamma^2)^2}\left(1+\frac{\mathbf{q}^2(p^2-\gamma^2-2\eta p\gamma)}{2(p^2+\gamma^2)^2}\right)\times\left(\frac{2\pi\eta}{e^{2\pi\eta}-1}\right)e^{4\eta\tan^{-1}(p/\gamma)},$$

$$F_2=\frac{4M_N\gamma p}{\pi(p^2+\gamma^2)^2}\left(1-\frac{\mathbf{q}^2(p^2+3\gamma^2+6\eta p\gamma)}{6(p^2+\gamma^2)^2}\right)\times\left(\frac{2\pi\eta}{e^{2\pi\eta}-1}\right)e^{4\eta\tan^{-1}(p/\gamma)}, \quad \text{(B22)}$$

$$F_4=\frac{1}{\pi}\mathrm{Im}[{B_0}^2({A_{-1}}^{(^1S_0,pp)}(p)+\epsilon{A_0}^{(^1S_0,pp)}(p)+\epsilon^2{A_1}^{(^1S_0,pp)}(p))],$$

$$B_0=M_N\int\frac{d^3k}{(2\pi)^3}\frac{\sqrt{8\pi\gamma}}{k^2+\gamma^2}\frac{2\pi\eta_k}{e^{2\pi\eta_k}-1}\frac{e^{2\eta_k\tan^{-1}(k/\gamma)}}{p^2-k^2+i\epsilon}\times\left[1+\frac{\mathbf{q}^2((1-2\eta_k^2)k^2-6\eta_k k\gamma-3\gamma^2)}{12(q^2+\gamma^2)^2}\right], \quad \text{(B23)}$$

$$\eta=\frac{\alpha M_N}{2p},\quad \eta_k=\frac{\alpha M_N}{2k},$$

$$p=\sqrt{M_N(\nu-m_n+m_p)-\gamma^2-\frac{\mathbf{q}^2}{4}+i\epsilon}, \quad \text{(B24)}$$

$$C_V^{(1)}=\frac{|V_{ud}|}{\sqrt{2}},\quad C_A^{(1)}=\frac{|V_{ud}|}{\sqrt{2}}g_A,\quad C_M^{(1)}=\sqrt{2}|V_{ud}|\kappa^{(1)},$$

$$G_2=-\epsilon\frac{M_N}{3\pi^2}\mathrm{Im}\left[\sqrt{\frac{\gamma}{2\pi}}B_0C_A^{(1)}\tilde{L}_{1,A}({A_{-1}}^{(^1S_0,pp)}(p)+\epsilon{A_0}^{(^1S_0,pp)}(p))\right]+\epsilon^2\frac{M_N^2\gamma}{96\pi^4}\mathrm{Im}[\tilde{L}_{1,A}^2{A_{-1}}^{(^1S_0,pp)}(p)], \quad \text{(B25)}$$

$$G_3=\epsilon^2\frac{M_N}{3\pi^2}\mathrm{Im}\left[\sqrt{\frac{\gamma}{2\pi}}B_0(C_M^{(1)}\tilde{L}_{1,A}+C_A^{(1)}\tilde{L}_{1,M}){A_{-1}}^{(^1S_0,pp)}(p)\right].$$

$$\tilde{L}_{1,A}=-\frac{4\pi(\mu-\gamma)}{M_N C_{0,-1}^{(^1S_0,pp)}}\left[\sqrt{2}|V_{ud}|L_{1,A}-2\pi C_A^{(1)}\left(\frac{M_N}{2\pi}C_{2,-2}^{(^1S_0,pp)}+\frac{\rho_d}{(\mu-\gamma)^2}\right)\right], \quad \text{(B26)}$$

$$\tilde{L}_{1,M}=-\frac{8\pi(\mu-\gamma)}{M_N C_{0,-1}^{(^1S_0,pp)}}\left[\sqrt{2}|V_{ud}|M_N L_1-\pi C_M^{(1)}\left(\frac{M_N}{2\pi}C_{2,-2}^{(^1S_0,pp)}+\frac{\rho_d}{(\mu-\gamma)^2}\right)\right],$$

evaluated at $\mu=m_\pi$, with $C_{0,-1}^{(^1S_0,pp)}=-3.77$ fm^2 and $C_{2,-2}^{(^1S_0,pp)}=7.50$ fm^4.

[1] G.T. Ewan *et al.*, SNO proposal No. SNO-87-12, 1987.
[2] G.A. Aardsma *et al.*, Phys. Lett. B **194**, 321 (1987).
[3] F. T. Avignone and Yu. V. Efremenko, in *Proceedings of the 2000 Carolina Conference on Neutrino Physics*, edited by K. Kubodera (World Scientific, Singapore, 2000).
[4] S.D. Ellis and J.N. Bahcall, Nucl. Phys. **A114**, 636 (1968).
[5] A. Ali and C.A. Dominguez, Phys. Rev. D **12**, 3673 (1975).
[6] H.C. Lee, Nucl. Phys. **A294**, 473 (1978).
[7] J.N. Bahcall, K. Kubodera, and S. Nozawa, Phys. Rev. D **38**, 1030 (1987).
[8] N. Tatara, Y. Kohyama, and K. Kubodera, Phys. Rev. C **42**, 1694 (1990).
[9] M. Doi and K. Kubodera, Phys. Rev. C **45**, 1988 (1992).
[10] K. Kubodera and S. Nozawa, Int. J. Mod. Phys. E **3**, 101 (1994); Y. Kohyama and K. Kubodera, USC(NT)-Report-92-1, 1992.
[11] S. Ying, W.C. Haxton, and E.M. Henley, Phys. Rev. C **45**, 1982 (1992); Phys. Rev. D **40**, 3211 (1989).
[12] S. Nakamura, T. Sato, V. Gudkov, and K. Kubodera, nucl-th/0009012.
[13] M.N. Butler and J.W. Chen, Nucl. Phys. **A675**, 575 (2000).
[14] D.B. Kaplan, M.J. Savage, and M.B. Wise, Phys. Lett. B **424**, 390 (1998); Nucl. Phys. **B534**, 329 (1998); Phys. Rev. C **59**, 617 (1999).
[15] T.D. Cohen and J.M. Hansen, Phys. Rev. C **59**, 13 (1999).
[16] G. Rupak and N. Shoresh, Phys. Rev. C **60**, 054004 (1999).
[17] D.B. Kaplan and J.V. Steele, Phys. Rev. C **60**, 064002 (1999).
[18] S. Fleming, T. Mehen, and I.W. Stewart, Phys. Rev. C **61**, 044005 (2000); Nucl. Phys. **A677**, 313 (2000).
[19] J.W. Chen, G. Rupak, and M.J. Savage, Nucl. Phys. **A653**, 386 (1999).
[20] D.B. Kaplan, M.J. Savage, and M.B. Wise, Nucl. Phys. **B478**, 629 (1996).
[21] D.B. Kaplan, Nucl. Phys. **B494**, 471 (1997).
[22] T.D. Cohen, Phys. Rev. C **55**, 67 (1997); D.R. Phillips and T.D. Cohen, Phys. Lett. B **390**, 7 (1997); S.R. Beane, T.D. Cohen, and D.R. Phillips, Nucl. Phys. **A632**, 445 (1998).
[23] M. Luke and A. Manohar, Phys. Rev. D **55**, 4129 (1997).
[24] G.P. Lepage, nucl-th/9706029.
[25] U. van Kolck, hep-ph/9711222; Nucl. Phys. **A645**, 273 (1999).

[26] P.F. Bedaque and U. van Kolck, Phys. Lett. B **428**, 221 (1998); P.F. Bedaque, H.W. Hammer, and U. van Kolck, Phys. Rev. Lett. **82**, 463 (1999).
[27] J.W. Chen and M.J. Savage, Phys. Rev. C **60**, 065205 (1999); J.W. Chen, G. Rupak, and M.J. Savage, Phys. Lett. B **464**, 1 (1999).
[28] G. Rupak, nucl-th/9911018.
[29] X. Kong and F. Ravndal, Phys. Lett. B **450**, 320 (1999); Nucl. Phys. **A656**, 421 (1999); **A665**, 137 (2000); nucl-th/0004038.
[30] M.J. Savage and J. Walden, Phys. Rev. D **55**, 5376 (1997).
[31] D.B. Kaplan and A. Manohar, Nucl. Phys. **B310**, 527 (1988).
[32] B. Mueller *et al.*, Phys. Rev. Lett. **78**, 3824 (1997).
[33] M. Pitt (private communication).
[34] G.A. Miller and W.T.H. Van Oers, nucl-th/9409013.
[35] T. Sato, S. Nakamura, and K. Kubodera (private communication).
[36] R.B. Wiringa, V.G.J. Stoks, and R. Schiavilla, Phys. Rev. C **51**, 38 (1995).